A (2 mg ml^{-1}) at 37 °C for 40 min. After filtration through sieve membranes (with 100 μm pores), tumour cells were immunosorted using an epithelial specific antigen (Ep-CAM) antibody bound to Dynal™ beads (Dynal, Oslo, Norway) following the vendor's instructions (Nakayama *et al*, 2006). Freshly isolated tumour cells were allowed to grow in culture and were used for experiments within two passages.

Mutational analysis of *KRAS* and *BRAF*

Genomic DNA was purified from all the cell lines and formalin-fixed, paraffin-embedded tissues using a Qiaquick polymerase chain reaction (PCR) purification kit (Qiagen, Valencia, CA, USA). PCR was then carried out followed by nucleotide sequencing using the iCycler (Bio-Rad, Hercules, CA, USA). Exon 1 of *KRAS* and exon 15 of *BRAF* were both sequenced, as these mutational hot spots together harbour nearly all published mutations (Davies *et al*, 2002; Singer *et al*, 2002, 2003; Sieben *et al*, 2004). The primers for PCR and sequencing were manufactured by GeneLink (Hawthorne, NY, USA), and their sequences were described in an earlier report (Nakayama *et al*, 2006). The sequences were analysed using the Lasergene programme, DNASTAR (Madison, WI, USA).

Immunohistochemistry

Expression of the active phosphorylated ERK1/2 (p-ERK1/2) was assessed by immunohistochemistry and western blot analysis. The antibody used in this study was a rabbit polyclonal antibody that reacted with phosphorylated but not unphosphorylated ERK1/2 (Cell Signaling Technology). Immunohistochemistry was carried out on tissue microarrays at a dilution of 1 : 1000 followed by detection with the En Vision + System using the peroxidase method (DAKO, Carpinteria, CA, USA). The percentage of positive cells was estimated by randomly counting ~500 tumour cells from three different high-power fields (× 40) within one specimen. A positive reaction was defined as a discrete localisation of the brown chromagen in the nucleus or cytoplasm. Cases in which more than 5% of the tumour cells showed detectable immunoreactivity were scored as positive.

Western blot analysis

Cell lysates were prepared by dissolving cell pellets in Laemmli sample buffer (BioRad, Hercules, CA, USA) supplemented with 5% β-mercaptoethanol (Sigma, St Louis, MO, USA). Western blot analysis was performed on ovarian cancer/OSE cell lines/cultures, including OVCAR3, SKOV3, A2780, MDAH2774, ES2, MPSC1, KF28, OVK#18, OMC3, JHOC5, PC1, PC2, PC3, IOSE29, OSE7, and OSE10. Similar amounts of total protein from each lysate were loaded and separated on 10% Tris-Glycine-SDS polyacrylamide gels (Novex, San Diego, CA, USA) and electroblotted to Millipore Immobilon-P polyvinylidene difluoride membranes. The membranes were probed with an active ERK1/2 antibody (pTEpY, 1 : 5000) (Cell Signaling Technology) followed by a peroxidase-conjugated anti-mouse or anti-rabbit immunoglobulin (1 : 20 000). The same membrane was probed with an antibody that reacted with total ERK1/2 (1 : 5000) (Cell Signaling Technology) for loading controls. Western blots were developed by chemiluminescence (Pierce, Rockford, IL, USA).

Cell-growth assays

For the cell-growth assay, cells were plated at the same density (3×10^3 cells per well) in 96-well plates. An methyl thiazoyl tetrazorium (MTT) cell-growth assay was performed (Nakayama *et al*, 2001) 96 h after treating the cells with CI-1040 (provided by Pfizer, Inc., New York, NY, USA) at 5 μM or with dimethyl sulphoxide (DMSO) (control). The data were expressed as a percentage of the DMSO control. The mean and standard deviation (s.d.) were obtained from three experiments. Apoptotic cells were detected with 4',6-diamidino-2-phenylindole (DAPI) staining. The data were expressed as the mean ± 1 s.d. from triplicates. To confirm the presence of apoptotic cells, DAPI-stained cells were also stained with Annexin V dye. Bromodeoxyuridine (BrdUrd) uptake and staining were measured using a cell proliferation kit (Amersham, Buckinghamshire, England, UK) and apoptotic cells were detected using an Annexin V staining kit (Bio Vision, Mountain View, CA, USA). The percentages of BrdUrd-positive and Annexin V-positive cells were determined by counting approximately 400 cells from each well in 96-well plates. The data were expressed as the mean ± 1 s.d. of triplicates.

Tumour xenograft in nude mice

To confirm the findings of a CI-1040 effect *in vitro*, we injected 3×10^6 MDAH2774 or SKOV3 cells into the intraperitoneal tissue of *nu/nu* mice (4 weeks of age). Four weeks BALB/c *nu/nu* mice were purchased from Charles River Japan Inc. (Kanagawa, Japan). CI-1040 was prepared in a vehicle of 10% Cremophore EL (Sigma, St Louis, MO, USA), 10% ethanol, and 80% water. When the model for the mouse study was first designed, the end point was set to be the day when the mice began to produce ascites, or acute gain of weight due to tumour growth, for reasons of ethical origin. Tumours that start causing ascites have a chance of developing other malignant characteristics, which can become harmful progressively. Four mice were used for each experimental group. During the study, the mice were killed when it was discovered that the abdomen of one of the mice had begun to distend because of ascites. One week after tumour-cell injection, either CI-1040 (CI-1040, 150 mg kg^{-1}, resuspended in 10% Cremophore EL (Sigma), 10% ethanol, and 80% water) or a vehicle only (10% Cremophore EL (Sigma), 10% ethanol, and 80% water) were injected intraperitoneally (i.p.) once daily for 3 weeks. The total dose of CI-1040 for each mouse was 63 mg. Four weeks after the cell injection (three weeks after CI-1040 injection), the abdomens of the control group mice had begun to distend. The time for termination of the experiment was dictated by the aforementioned ethical reasons (tumour ascites in controls), and this endpoint was observed at that time. We anaesthetised the mice before they were rendered moribund by the experiment. The total tumour weight at that time was around 500 mg. Necropsy was carried out on all mice to assess i.p. tumour growth, and the tumours were excised and weighed. Animal experiments were carried out in accordance with the regulations of the Institutional Ethical Commission (Shimane University) and of the United Kingdom Co-ordinating Committee on Cancer Research guidelines (Workman, 1998).

Statistical methods for clinical correlation

Overall survival was calculated from the date of diagnosis to the date of death or last follow-up. Patients with either *KRAS* or *BRAF* mutations had similar performance status distributions. The data were plotted as Kaplan–Meier curves, and the statistical significance was determined by the log-rank test. Data were censored when patients were lost to follow-up. The Student's *t*-test was used to examine the statistical significance in the difference of growth-assay data.

RESULTS

Identification of *KRAS* and *BRAF* mutations

The mutational status of *KRAS* and *BRAF* in all 45 ovarian carcinomas is summarised in Table 1. Somatic mutations of *KRAS* were identified in 8 (13.7%) out of 58 ovarian carcinomas. In

contrast, somatic mutations of *BRAF* were identified in 5 (8.6%) out of 58 ovarian carcinomas. Somatic mutations of either *KRAS* or *BRAF* were identified in 12 (20.6%) out of 58 ovarian carcinomas. Most *KRAS* mutations were located at codon 12 and all *BRAF* mutations at codon 600. Both of these codons are mutation hot spots. Interestingly, simultaneous mutations of *KRAS* and *BRAF* did not occur in the tested ovarian carcinomas with the exception of one mucinous case.

A panel of ovarian cancer cell lines and primary cultures was first analysed for tumour mutation status in the *KRAS* and *BRAF* genes. As shown in Figure 1, three ovarian cancer cell lines harboured either *KRAS* or *BRAF* mutations. The frequency of either *KRAS* or *BRAF* mutations in conventional serous high-grade carcinomas (4.0%: 1/25) was significantly lower than in the other histological type (32.2%: 10/31).

Relationship between *KRAS/BRAF* mutations and p-ERK1/2 expression or clinicopathological factors

The immunoreactivity of active p-ERK1/2 was detected in both the nucleus and the cytoplasm of the tumour cells (Figure 2). This is consistent with an earlier report (Mizumoto *et al*, 2007). Positive active p-ERK1/2 was identified in 27 (46.6%) out of 58 ovarian carcinomas. The patients were stratified into two groups depending on the mutational status of *KRAS/BRAF*. The relationships between *KRAS/BRAF* mutations and clinicopathological factors, including p-ERK1/2 expression are shown in Table 2. There was no significant correlation between *KRAS/BRAF* mutations and the patient's age. The results in Table 2 show that *KRAS/BRAF* mutation is correlated significantly with FIGO stage I, II ($P<0.001$), and p-ERK1/2 ($P<0.001$). In addition, there were significant correlations between *KRAS/BRAF* mutations and pathological grade ($P=0.004$), and histological subtype ($P=0.014$).

Effect of *KRAS/BRAF* mutations or p-ERK1/2 on the prognosis of ovarian carcinomas

Next, we examined the prognostic effect of *KRAS/BRAF* mutations and p-ERK1/2 expression. Out of the 58 samples that we examined, 45 were available for prognostic analysis. Kaplan–Meier estimates of overall survival are plotted in Figure 3. There was no significant relationship between *KRAS/BRAF* mutations or p-ERK1/2 expression and overall survival in patients with ovarian carcinoma ($P=0.2460$, $P=0.9339$, respectively). Univariate analysis showed that only FIGO stage III, IV affected the overall survival of patients with ovarian carcinoma significantly($P=0.014$).

Effects of ERK1/2 inactivation on ovarian carcinoma *in vitro*

A panel of ovarian cancer cell lines and primary cultures of ovarian cancer were first analysed for *KRAS* and *BRAF* gene mutation status. Mutational status was correlated with growth inhibition and apoptosis induction by the MEK inhibitor CI-1040 that prevented activation of the downstream target, ERK1/2. Western blot analysis showed a dose-dependent effect on the expression of active ERK1/2 in ES2 cells, and active ERK1/2 was not detectable 6 h after treating the cells with CI-1040 at a concentration of 5 μM (Figure 4). As shown in Figure 5, four of the tumours harbouring either *KRAS* or *BRAF* mutations showed a marked reduction (<50% of DMSO control) in the cell number in the CI-1040-treated group as compared with the other 14 tumours containing wild-type *KRAS* and *BRAF* ($P<0.001$). CI-1040 had no significant effect on the growth of normal cells, including the OSE cells. It is likely that *KRAS/BRAF* mutation is not the only determinant for activating ERK1/2. Therefore, we analysed p-ERK1/2 expression in each of the cell lines listed in Figure 5. Only four of these cell lines, MDAH2774, ES2, MPSC1, and POC1, strongly expressed p-ERK1/2. SKOV3 and A2780 showed weak expression of ERK1/2.These results suggest that activation of ERK1/2 may depend on *KRAS/BRAF* mutation in ovarian cancer cells.

To assess the mechanisms underlying growth inhibition by CI-1040, we measured the percentages of BrdUrd-labelled cells and Annexin V-labelled cells to estimate proliferation and apoptosis, respectively. We found that CI-1040 significantly reduced cellular proliferation and induced apoptosis in cell lines with either *KRAS* or *BRAF* mutations in comparison with cell lines with wild-type sequences (Figure 6, Supplementary Figure 1).

Effects of CI-1040 ERK1/2 inactivation on ovarian carcinomas *in vivo*

On the basis of the above findings, we investigated whether CI-1040 had a growth-inhibitory effect on tumour formation and development *in vivo*. Tumour xenografts from both MDAH2774 (*KRAS* mutant) and SKOV3 (wild type of *KRAS* and *BRAF*) cell

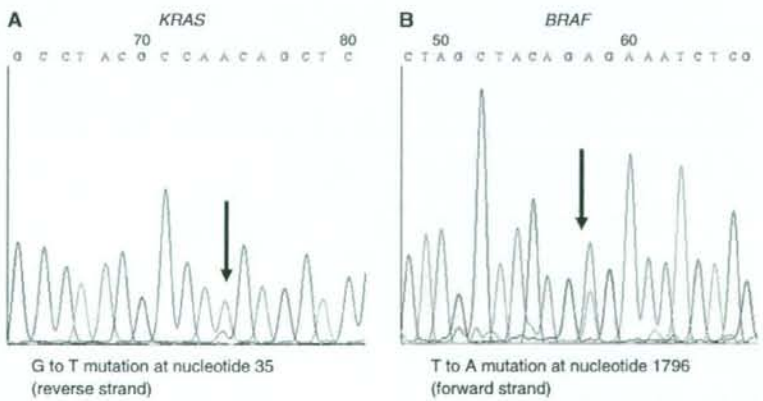

Figure 1 Chromatograms of *KRAS* and *BRAF* mutational status in three representative ovarian cancer cells. (**A**) Left panel (MDAH2774) showing a point mutation in the *KRAS* gene. (**B**) Right panel (ES2) showing a point mutation in the *BRAF* gene. Arrows represent spike which indicates mutation.

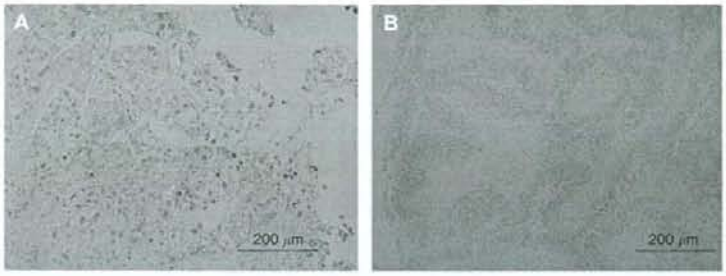

Figure 2 Immunohistochemical staining of phosphorylated extracellular-regulated kinase (p-ERK1/2). (**A**) Intense immunoreactivity is present in both the nucleus and the cytoplasm in this ovarian carcinoma. (**B**) A case with negative staining of phosphorylated ERK1/2 (p-ERK1/2).

Table 2 Association between *KRAS/BRAF* mutational status and clinicopathological factors in patients with ovarian cancer

		KRAS/BRAF mutation		
Factors	**Patients**	**Negative**	**Positive**	***P*-value**
FIGO stage				
I, II	18	8	10	<0.001
III, IV	38	38	2	
Grade				
G1	9	3	6	<0.001
G2, G3	49	43	6	
Histology				
Serous	28	26	2	0.014
Others	30	20	10	
Age (years)				
<60	35	28	7	0.293
≥60	23	17	6	
p-ERK1/2				
Positive	27	15	12	<0.001
Negative	31	31	0	

FIGO, International Federation of Gynecology and Obstetrics; MAPK, mitogen-activated protein kinase; ERKV2, Extracellular signal-regulated protein kinases1/2.

lines were established in a *nu/nu* mouse model. All mice injected with CI-1040 developed significantly smaller intra-abdominal xenograft tumours than the mice carrying diluent control cells of the *KRAS* mutant cell line MADH2774 (Figure 7A). There were no differences in intra-abdominal xenograft tumour weights between the CI-1040-treated group and control groups transplanted with the wild-type *KRAS/BRAF* cell line SKOV3 (Figure 7B). Histological examination of the tumours after CI-1040 treatment showed inactivation of p-ERK1/2 in tumour cells based on immunohistochemistry (Figure 7C and D).

DISCUSSION

The significantly higher frequency of *KRAS/BRAF* mutations in non-serous type carcinomas compared with conventional high-grade serous carcinomas in this study is a finding of great interest. It suggests that conventional high-grade serous and non-serous tumours may be distinguished on the basis of characteristic genetic alterations. In addition, this observation further supports the theory that ovarian carcinoma arises from multiple pathways (Shih Ie and Kurman, 2004, 2005). In this model, conventional high-grade serous and non-serous carcinomas develop independently from one another and are characterised by different molecular genetic changes and gene expression profiles (Schwartz *et al*, 2002; Marquez *et al*, 2005).

We reported earlier that *KRAS* or *BRAF* mutations were quite common in low-grade serous ovarian carcinomas but rare in conventional high-grade serous carcinomas (Nakayama *et al*, 2006). Our present results showing low frequencies of either *KRAS* or *BRAF* mutations in conventional high-grade serous carcinoma are consistent with our earlier reports (Nakayama *et al*, 2006).

V600E is the most common *BRAF* mutation in ovarian cancer (Singer *et al*, 2003; Sieben *et al*, 2004; Shih Ie and Kurman, 2005; Nakayama *et al*, 2006). However, mutations at E585K and G463E have also been reported in ovarian cancer samples and cell lines (Davies *et al*, 2002). Therefore, further studies are needed to clarify the effects of other *BRAF* mutations in ovarian cancer, and to completely describe the mutation profile of *KRAS-BRAF* signalling in established ovarian cancer cell lines.

In this study, we also showed that the ERK–MAPK pathway was activated in 15 (33.3%) out of 45 ovarian carcinomas and activation depended on the mutational status of *KRAS* and *BRAF*. This is in contrast with a recent report showing that this pathway is frequently activated independent of the status of *KRAS* and *BRAF* in endometrioid-type endometrial cancer (Mizumoto *et al*, 2007). This discrepancy may be because of differences in organ-specific oncogenic pathways. The RAS–RAF–MEK–ERK pathway may play an important role in ovarian carcinogenesis but not in endometrial carcinogenesis. Similarly, alternative pathways for ERK activation, such as crosstalk with the PI3K pathway, exist in endometrial cancer but are rare in ovarian cancer. Indeed, PI3K signalling by either *PIK3CA* or *PTEN* mutations occurs in 40% of endometrial cancers but in <5% of ovarian cancers (Tashiro *et al*, 1997; Oda *et al*, 2005; Kolasa *et al*, 2006; Nakayama *et al*, 2006).

In this study, *KRAS /BRAF* mutations tended to have a favourable but not statistically significant effect on overall survival. Our findings contrast with a recent report showing a positive correlation between a *KRAS* or *BRAF* mutation and clinical aggressiveness in colorectal, non-small-cell lung, and thyroid cancers (Lievre *et al*, 2006; Lee *et al*, 2007; Massarelli *et al*, 2007). This difference in prognostic significance between ovarian cancer and the latter types is intriguing, and it probably reflects organ-specific roles of the *KRAS/BRAF* pathway. In this study, 8 out of 9 *KRAS/BRAF* mutations were identified in early stage (stage I, II) tumours. This may reflect a more indolent course of tumours with *KRAS/BRAF* mutations.

In an earlier report, advanced ovarian cancer patients (stage III, IV) with p-ERK expression had a longer overall survival than patients with low p-ERK values (Hsu *et al*, 2004). However, we did not find a significant correlation between p-ERK expression and overall survival in our study. This difference may be because of a

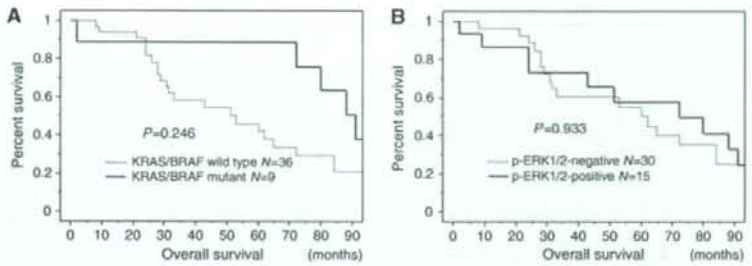

Figure 3 Kaplan–Meier survival curve in 45 patients with ovarian carcinoma according to *KRAS/BRAF* mutation and phosphorylated ERK (p-ERK) expression. (**A**) KRAS/BRAF mutational status correlates with favourable overall survival in patients with ovarian carcinoma. (**B**) p-ERK1/2 expression does not correlate with shorter overall survival in patients with ovarian carcinoma.

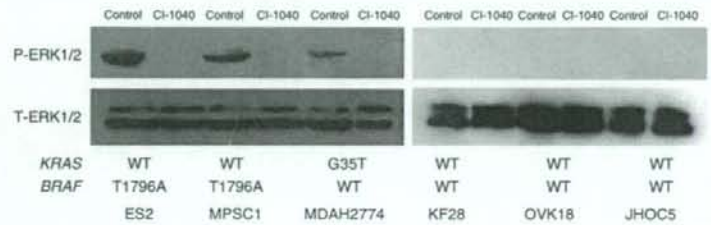

Figure 4 Western blot analysis. Expression of phosphorylated ERK1/2 (p-ERK1/2) is undetectable in all CI-1040-treated samples. A similar amount of protein was loaded in CI-1040 and DMSO-treated samples as evidenced by a similar intensity of total ERK1/2. D, DMSO treatment, C, and CI-1040 treatment.

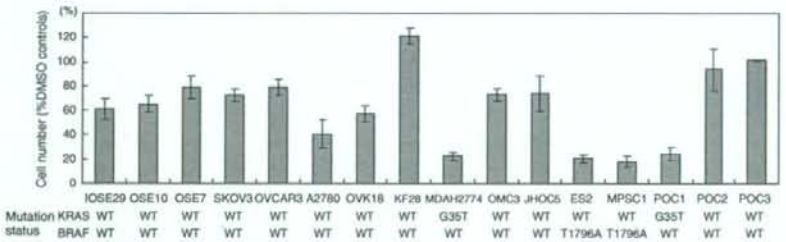

Figure 5 Effects of CI-1040 on cell proliferation. Cells were counted after 72 h of CI-1040 or DMSO (control) treatment. The mutational status of *KRAS* and *BRAF* for each sample is shown under the cell lines and primary cancer cell cultures. Ovarian cancers with mutations in either *KRAS* or *BRAF* are more sensitive to growth inhibition by CI-1040 than those with wild-type (WT) sequences.

higher percentage of early-stage ovarian cancers and endometrioid and mucinous histology tumours being included in this study as compared with the earlier study.

Although the biological roles of the RAS–RAF–MEK–ERK pathways in human cancer have been thoroughly investigated, there have been no recent studies. Therefore, it is not known whether the activation of *KRAS* or *BRAF* mutations alters the effects of these pathways on tumour progression. In this study, we carried out a genotype–phenotype correlation of ovarian cancer cells using a MEK inhibitor, CI-1040. In this study, we focussed on CI-1040 because it inhibited the common downstream target in the RAS signalling pathway. Therefore, CI-1040 has the potential to be developed into a drug for the treatment of ovarian carcinomas in patients with either *KRAS* or *BRAF* mutations. An oral formulation of CI-1040 had already been shown to be an effective MEK inhibitor and was generally well tolerated in a multicentre phase II study (Rinehart *et al*, 2004). Our results provide compelling evidence that the biological effects of the ERK signalling pathway depend on the mutational status of its upstream regulators, (i.e.), the *KRAS* and *BRAF* genes. Ovarian carcinomas with mutations in either *KRAS* or *BRAF* were more sensitive to growth inhibition and apoptosis induction by the MEK inhibitor, CI-1040. This observation suggests that ovarian carcinomas with mutations in either *KRAS* or *BRAF* are more highly dependent on the activation of the RAS–RAF–MEK–ERK pathway for cell proliferation and survival than those without such mutations. Thus, inactivation of ERK1/2 results in marked growth inhibition in ovarian carcinomas with mutations in *KRAS* or *BRAF* in comparison with only a modest effect on wild-type tumours. The above observations lend strong support to the view of 'kinase addiction' by which the activating mutations in the kinase pathway confer susceptibility of the tumours to an inhibitor (Sebolt-Leopold *et al*, 1999; Arteaga and Baselga, 2004). In microsatellite-unstable colorectal cancer cell lines, the effect of BRAF inhibition depended on whether the cell harboured a *BRAF* or a *KRAS* mutation. *BRAF* inhibition by small interfering RNA resulted in significantly decreased proliferation and increased apoptosis in the *BRAF* mutant lines. In contrast, this effect was not seen in the *KRAS* mutant lines (Preto *et al*, 2008). Cells carrying *BRAF* mutations have also been shown to be more sensitive to

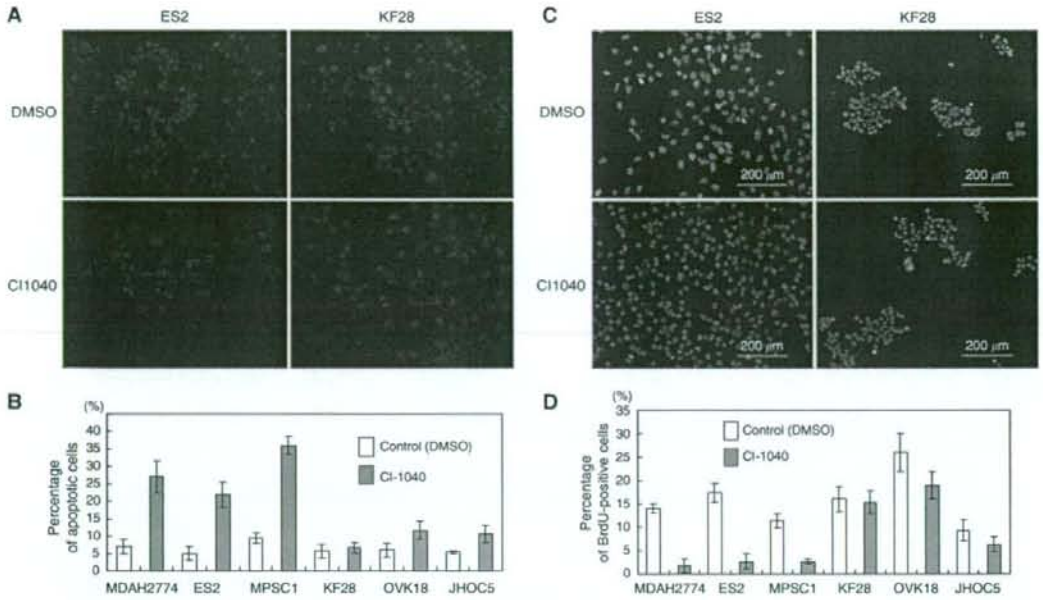

Figure 6 Detection of apoptotic cells and proliferation cells. (**A**) The CI-1040-treated ES2 cells, but not KF28 cells, show morphological features typical of apoptosis. (**B**) Apoptotic cells are quantified by counting them under a fluorescent microscope. (**C**) Treatment with CI-1040 decreases DNA synthesis as measured by BrdUrd uptake in ES2 cells, but not KF28 cells. (**D**) Proliferation is estimated by counting BrdUrd-stained cells under a fluorescent microscope. The experiment was performed 72 h after CI-1040 or DMSO treatment.

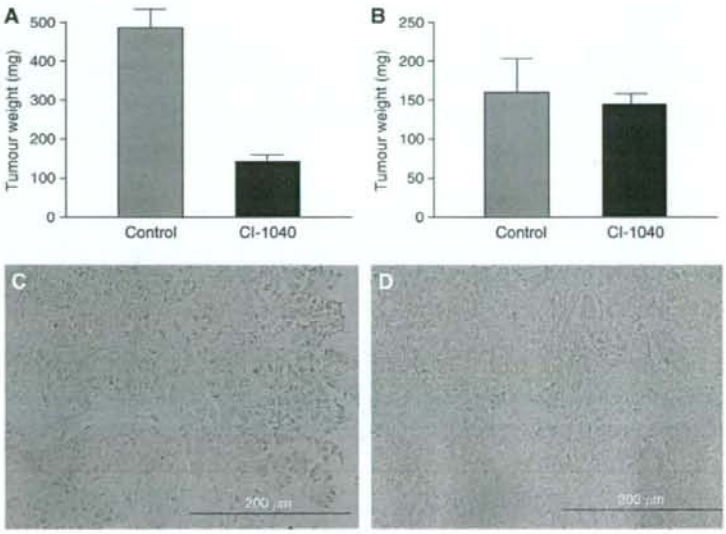

Figure 7 Effects of CI-1040 in a mouse xenograft model. (**A**) CI-1040-treated cells produced small tumour nodules in the peritoneal cavity. However, the diluent control-treated cells grew much larger i.p. tumours in *KRAS* mutant MDAH2774 cells. (**B**) In contrast, there were no differences in tumour weights between CI-1040-treated cells and control-treated cells in wild-type (WT) *KRAS/BRAF* SKOV3 cells. Tumours were excised and weighed. The data are expressed as the total tumour weight from each mouse. (**C** and **D**) Immunohistochemical staining of phosphorylated extracellular-regulated kinase 1/2 (p-ERK1/2) in tumours with *KRAS* mutant MDAH2774 cells. (**C**) Intense immunoreactivity is present in both the nucleus and the cytoplasm in CI-1040-untreated tumour. (**D**) Immunoreactivity is absent in both the nucleus and the cytoplasm in CI-1040-untreated tumour cells.

MEK inhibitors than cells with *RAS* mutations (Solit *et al*, 2006). This raises the possibility that *KRAS* and *BRAF* mutant cancer cells might be differentially dependent on signalling mechanisms that involve MEK. This difference in sensitivity to the RAS–RAF–MEK–ERK pathway between ovarian cancer and the latter types is intriguing, and it probably reflects organ-specific roles of the *KRAS and BRAF* oncogenes.

In light of our *in vivo* and *in vitro* findings, we propose that ovarian cancer patients with *KRAS* or *BRAF* mutations be considered for MEK inhibitor (CI-1040) therapy if they recur after conventional platinum and taxane chemotherapy.

Thus far, the MEK inhibitor CI-1040 has fared poorly in clinical trials for breast, colon, and lung cancer (Rinehart *et al*, 2004). However, its favourable therapeutic index and high selectivity may outweigh its shortcomings in *KRAS* and *BRAF* mutant ovarian cancer. Therefore, we recommend that in further clinical trials of MEK inhibitors for ovarian cancer, patients are stratified on the basis of *KRAS/BRAF* mutational status.

In summary, we have shown that the phenotypic change in ovarian carcinomas in response to ERK1/2 inactivation depends on the mutational status of *KRAS and BRAF*. The findings in this study provide new insight into the biological roles of the RAS–RAF–MEK–ERK signalling pathway in ovarian carcinomas. In addition, our observations have an important therapeutic implication in ovarian cancer patients with *KRAS* or *BRAF* mutations. Ovarian carcinomas with *KRAS* or *BRAF* mutation are clinically low-grade carcinomas of serous or other histological subtypes that are often refractory to conventional cytotoxic chemotherapy (Bristow *et al*, 2002a, b; Winter *et al*, 2007). Therefore, detection of *KRAS* and *BRAF* mutations in ovarian cancers may identify patients who will benefit from CI-1040 therapy.

ACKNOWLEDGEMENTS

This study is supported by grants from the Ministry of Education, Culture, Sports, Science and Technology in Japan, and the Japan Society of Gynecologic Oncology.

Supplementary Information accompanies the paper on British Journal of Cancer website (http://www.nature.com/bjc)

REFERENCES

Allen LF, Sebolt-Leopold J, Meyer MB (2003) CI-1040 (PD184352), a targeted signal transduction inhibitor of MEK (MAPKK). *Semin Oncol* **30:** 105–116

Arteaga CL, Baselga J (2004) Tyrosine kinase inhibitors: why does the current process of clinical development not apply to them? *Cancer Cell* **5:** 525–531

Bristow RE, Gossett DR, Shook DR, Zahurak ML, Tomacruz RS, Armstrong DK, Montz FJ (2002a) Micropapillary serous ovarian carcinoma: surgical management and clinical outcome. *Gynecol Oncol* **86:** 163–170

Bristow RE, Gossett DR, Shook DR, Zahurak ML, Tomacruz RS, Armstrong DK, Montz FJ (2002b) Recurrent micropapillary serous ovarian carcinoma. *Cancer* **95:** 791–800

Brose MS, Volpe P, Feldman M, Kumar M, Rishi I, Gerrero R, Einhorn E, Herlyn M, Minna J, Nicholson A, Roth JA, Albelda SM, Davies H, Cox C, Brignell G, Stephens P, Futreal PA, Wooster R, Stratton MR, Weber BL (2002) BRAF and RAS mutations in human lung cancer and melanoma. *Cancer Res* **62:** 6997–7000

Davies H, Bignell GR, Cox C, Stephens P, Edkins S, Clegg S, Teague J, Woffendin H, Garnett MJ, Bottomley W, Davis N, Dicks E, Ewing R, Floyd Y, Gray K, Hall S, Hawes R, Hughes J, Kosmidou V, Menzies A, Mould C, Parker A, Stevens C, Watt S, Hooper S, Wilson R, Jayatilake H, Gusterson BA, Cooper C, Shipley J, Hargrave D, Pritchard-Jones K, Maitland N, Chenevix-Trench G, Riggins GJ, Bigner DD, Palmieri G, Cossu A, Flanagan A, Nicholson A, Ho JW, Leung SY, Yuen ST, Weber BL, Seigler HF, Darrow TL, Paterson H, Marais R, Marshall CJ, Wooster R, Stratton MR, Futreal PA (2002) Mutations of the BRAF gene in human cancer. *Nature* **417:** 949–954

Gorden A, Osman I, Gai W, He D, Huang W, Davidson A, Houghton AN, Busam K, Polsky D (2003) Analysis of BRAF and N-RAS mutations in metastatic melanoma tissues. *Cancer Res* **63:** 3955–3957

Hsu CY, Bristow R, Cha MS, Wang BG, Ho CL, Kurman RJ, Wang TL, Shih Ie M (2004) Characterization of active mitogen-activated protein kinase in ovarian serous carcinomas. *Clin Cancer Res* **10:** 6432–6436

Kolasa IK, Rembiszewska A, Janiec-Jankowska A, Dansonka-Mieszkowska A, Lewandowska AM, Konopka B, Kupryjanczyk J (2006) PTEN mutation, expression and LOH at its locus in ovarian carcinomas. Relation to TP53, K-RAS and BRCA1 mutations. *Gynecol Oncol* **103:** 692–697

Lee JH, Lee ES, Kim YS (2007) Clinicopathologic significance of BRAF V600E mutation in papillary carcinomas of the thyroid: a meta-analysis. *Cancer* **110:** 38–46

Lievre A, Bachet JB, Le Corre D, Boige V, Landi B, Emile JF, Cote JF, Tomasic G, Penna C, Ducreux M, Rougier P, Penault-Llorca F, Laurent-Puig P (2006) KRAS mutation status is predictive of response to cetuximab therapy in colorectal cancer. *Cancer Res* **66:** 3992–3995

Marquez RT, Baggerly KA, Patterson AP, Liu J, Broaddus R, Frumovitz M, Atkinson EN, Smith DI, Hartmann L, Fishman D, Berchuck A, Whitaker R, Gershenson DM, Mills GB, Bast Jr RC, Lu KH (2005) Patterns of gene expression in different histotypes of epithelial ovarian cancer correlate with those in normal fallopian tube, endometrium, and colon. *Clin Cancer Res* **11:** 6116–6126

Massarelli E, Varella-Garcia M, Tang X, Xavier AC, Ozburn NC, Liu DD, Bekele BN, Herbst RS, Wistuba II (2007) KRAS mutation is an important predictor of resistance to therapy with epidermal growth factor receptor tyrosine kinase inhibitors in non-small-cell lung cancer. *Clin Cancer Res* **13:** 2890–2896

Mizumoto Y, Kyo S, Mori N, Sakaguchi J, Ohno S, Maida Y, Hashimoto M, Takakura M, Inoue M (2007) Activation of ERK1/2 occurs independently of KRAS or BRAF status in endometrial cancer and is associated with favorable prognosis. *Cancer Sci* **98:** 652–658

Nakayama K, Miyazaki K, Kanzaki A, Fukumoto M, Takebayashi Y (2001) Expression and cisplatin sensitivity of copper-transporting P-type adenosine triphosphatase (ATP7B) in human solid carcinoma cell lines. *Oncol Rep* **8:** 1285–1287

Nakayama K, Nakayama N, Kurman RJ, Cope L, Pohl G, Samuels Y, Velculescu VE, Wang TL, Shih Ie M (2006) Sequence mutations and amplification of PIK3CA and AKT2 genes in purified ovarian serous neoplasms. *Cancer Biol Ther* **5:** 779–785

Oda K, Stokoe D, Taketani Y, McCormick F (2005) High frequency of coexistent mutations of PIK3CA and PTEN genes in endometrial carcinoma. *Cancer Res* **65:** 10669–10673

Oliveira C, Velho S, Moutinho C, Ferreira A, Preto A, Domingo E, Capelinha AF, Duval A, Hamelin R, Machado JC, Schwartz Jr S, Carneiro F, Seruca R (2007) KRAS and BRAF oncogenic mutations in MSS colorectal carcinoma progression. *Oncogene* **26:** 158–163

Olson JM, Hallahan AR (2004) p38 MAP kinase: a convergence point in cancer therapy. *Trends Mol Med* **10:** 125–129

Peyssonnaux C, Eychene A (2001) The Raf/MEK/ERK pathway: new concepts of activation. *Biol Cell* **93:** 53–62

Pohl G, Ho CL, Kurman RJ, Bristow R, Wang TL, Shih Ie M (2005) Inactivation of the mitogen-activated protein kinase pathway as a potential target-based therapy in ovarian serous tumors with KRAS or BRAF mutations. *Cancer Res* **65:** 1994–2000

Preto A, Figueiredo J, Velho S, Ribeiro AS, Soares P, Oliveira C, Seruca R (2008) BRAF provides proliferation and survival signals in MSI colorectal carcinoma cells displaying BRAF(V600E) but not KRAS mutations. *J Pathol* **214:** 320–327

Rinehart J, Adjei AA, Lorusso PM, Waterhouse D, Hecht JR, Natale RB, Hamid O, Varterasian M, Asbury P, Kaldjian EP, Gulyas S, Mitchell DY, Herrera R, Sebolt-Leopold JS, Meyer MB (2004) Multicenter phase II study of the oral MEK inhibitor, CI-1040, in patients with advanced non-small-cell lung, breast, colon, and pancreatic cancer. *J Clin Oncol* **22:** 4456–4462

Schaeffer HJ, Weber MJ (1999) Mitogen-activated protein kinases: specific messages from ubiquitous messengers. *Mol Cell Biol* **19:** 2435–2444

Schwartz DR, Kardia SL, Shedden KA, Kuick R, Michailidis G, Taylor JM, Misek DE, Wu R, Zhai Y, Darrah DM, Reed H, Ellenson LH, Giordano TJ, Fearon ER, Hanash SM, Cho KR (2002) Gene expression in ovarian cancer reflects both morphology and biological behavior, distinguishing clear cell from other poor-prognosis ovarian carcinomas. *Cancer Res* **62:** 4722–4729

Sebolt-Leopold JS (2004) MEK inhibitors: a therapeutic approach to targeting the Ras-MAP kinase pathway in tumors. *Curr Pharm Des* **10:** 1907–1914

Sebolt-Leopold JS, Dudley DT, Herrera R, Van Becelaere K, Wiland A, Gowan RC, Tecle H, Barrett SD, Bridges A, Przybranowski S, Leopold WR, Saltiel AR (1999) Blockade of the MAP kinase pathway suppresses growth of colon tumors *in vivo*. *Nat Med* **5:** 810–816

Sebolt-Leopold JS, Van Becelaere K, Hook K, Herrera R (2003) Biomarker assays for phosphorylated MAP kinase. Their utility for measurement of MEK inhibition. *Methods Mol Med* **85:** 31–38

Shih Ie M, Kurman RJ (2004) Ovarian tumorigenesis: a proposed model based on morphological and molecular genetic analysis. *Am J Pathol* **164:** 1511–1518

Shih Ie M, Kurman RJ (2005) Molecular pathogenesis of ovarian borderline tumors: new insights and old challenges. *Clin Cancer Res* **11:** 7273–7279

Sieben NL, Macropoulos P, Roemen GM, Kolkman-Uljee SM, Jan Fleuren G, Houmadi R, Diss T, Warren B, Al Adnani M, De Goeij AP, Krausz T, Flanagan AM (2004) In ovarian neoplasms, BRAF, but not KRAS, mutations are restricted to low-grade serous tumours. *J Pathol* **202:** 336–340

Singer G, Kurman RJ, Chang HW, Cho SK, Shih Ie M (2002) Diverse tumorigenic pathways in ovarian serous carcinoma. *Am J Pathol* **160:** 1223–1228

Singer G, Oldt III R, Cohen Y, Wang BG, Sidransky D, Kurman RJ, Shih Ie M (2003) Mutations in BRAF and KRAS characterize the development of low-grade ovarian serous carcinoma. *J Natl Cancer Inst* **95:** 484–486

Solit DB, Garraway LA, Pratilas CA, Sawai A, Getz G, Basso A, Ye Q, Lobo JM, She Y, Osman I, Golub TR, Sebolt-Leopold J, Sellers WR, Rosen N (2006) BRAF mutation predicts sensitivity to MEK inhibition. *Nature* **439:** 358–362

Tashiro H, Blazes MS, Wu R, Cho KR, Bose S, Wang SI, Li J, Parsons R, Ellenson LH (1997) Mutations in PTEN are frequent in endometrial carcinoma but rare in other common gynecological malignancies. *Cancer Res* **57:** 3935–3940

Wan PT, Garnett MJ, Roe SM, Lee S, Niculescu-Duvaz D, Good VM, Jones CM, Marshall CJ, Springer CJ, Barford D, Marais R (2004) Mechanism of activation of the RAF-ERK signaling pathway by oncogenic mutations of B-RAF. *Cell* **116:** 855–867

Wingo PA, Tong T, Bolden S (1995) Cancer statistics, 1995. *CA Cancer J Clin* **45:** 8–30

Winter III WE, Maxwell GL, Tian C, Carlson JW, Ozols RF, Rose PG, Markman M, Armstrong DK, Muggia F, McGuire WP (2007) Prognostic factors for stage III epithelial ovarian cancer: a Gynecologic Oncology Group Study. *J Clin Oncol* **25:** 3621–3627

Workman P (1998) United Kingdom Co-ordinating Committee on Cancer Research (UKCCCR) Guidelines for the Welfare of Animals in Experimental Neoplasia (Second Edition). *Br J Cancer* **77:** 1–10

Yamamoto K, Kikuchi Y, Kudoh K, Nagata I (2000) Modulation of cisplatin sensitivity by taxol in cisplatin-sensitive and -resistant human ovarian carcinoma cell lines. *J Cancer Res Clin Oncol* **126:** 168–172

Available online at www.sciencedirect.com
ScienceDirect
Advanced Drug Delivery Reviews 60 (2008) 899–914
Advanced DRUG DELIVERY Reviews
www.elsevier.com/locate/addr

Poly (amino acid) micelle nanocarriers in preclinical and clinical studies ☆

Yasuhiro Matsumura *

Investigative Treatment Division, Research Center for Innovative Oncology, National Cancer Center Hospital East, 6-5-1 Kashiwanoha, Kashiwa City, 277-8577 Japan

Received 18 May 2007; accepted 15 November 2007
Available online 9 February 2008

Abstract

Polymeric micelles are expected to increase the accumulation of drugs in tumor tissues utilizing the EPR effect and to incorporate various kinds of drugs into the inner core by chemical conjugation or physical entrapment with relatively high stability. The size of the micelles can be controlled within the diameter range of 20 to 100 nm, to ensure that the micelles do not pass through normal vessel walls; therefore, a reduced incidence of the side effects of the drugs may be expected due to the decreased volume of distribution.

These are several anticancer agent-incorporated micelle carrier systems under clinical evaluation. Phase 1 studies of a CDDP incorporated micelle, Nc-6004, and an sN-38 incorporated micelle, NK012, are now underway. A phase 2 study of a PTX incorporated micelle, NK105, against stomach cancer is also underway.

Keywords: Poly (amino acid) micelle nanocarrier; Drug delivery system; EPR effect; Clinical trial

Contents

☆ This review is part of the *Advanced Drug Delivery Reviews* theme issue on "Clinical Developments in Drug Delivery Nanotechnology".

* Tel./fax: 81 4 7134 6857.

0169-409X/$ - see front matter © 2008 Elsevier B.V. All rights reserved.
doi:10.1016/j.addr.2007.11.010

1. Preface

Drug delivery system (DDS) could be used for active or passive targeting of tumor tissues. The former refers to the development of monoclonal antibodies directed against tumor-related molecules that allow targeting of the tumor, because of specific binding between the antibody and its antigen. However, the application of DDS using monoclonal antibodies is restricted to tumors expressing high levels of related antigens.

Passive targeting is based on the enhanced permeability and retention (EPR) effect [1]. The EPR effect is based on the pathophysiological characteristics of solid tumor tissues: hypervascularity, incomplete vascular architecture, secretion of vascular permeability factors stimulating extravasation within cancer tissue, and absence of effective lymphatic drainage from tumors that impedes the efficient clearance of macromolecules accumulated in solid tumor tissues.

Several techniques to maximally use the EPR effect have been developed, e.g., modification of drug structures and development of drug carriers. Polymeric micelle-based anticancer drugs were originally developed by Prof. Kataoka et al. in late the 1980s or early 1990s [2–4]. Polymeric micelles were expected to increase the accumulation of drugs in tumor tissues utilizing the EPR effect and to incorporate various kinds of drugs into the inner core by chemical conjugation or physical entrapment with relatively high stability. The size of the micelles can be controlled within the diameter range of 20 to 100 nm, to ensure that the micelles do not pass through normal vessel walls; therefore, a reduced incidence of the side effects of the drugs may be expected due to the decreased volume of distribution.

In this chapter, polymeric micelle systems for which clinical trials are now underway are reviewed.

2. NK105, paclitaxel-incorporating micellar nanoparticle

Paclitaxel(PTX) is one of the most useful anticancer agents known for various cancers, including ovarian, breast, and lung cancers [5,6]. However, PTX has serious adverse effects, e.g., neutropenia and peripheral sensory neuropathy. In addition, anaphylaxis and other severe hypersensitive reactions have been reported to develop in 2–4% of patients receiving the drug even after premedication with antiallergic agents; these adverse reactions have been attributed to the mixture of Cremophor EL and ethanol which was used to solubilize PTX [7,8]. Of the adverse reactions, neutropenia can be prevented or managed effectively by administering a granulocyte colony-stimulating factor. On the other hand, there are no effective therapies to prevent or reduce nerve damage which is associated with peripheral neuropathy caused by PTX; therefore, neurotoxicity constitutes a significant dose-limiting toxicity of the drug [9,10].

2.1. Preparation and characterization of NK105

To construct NK105 micellar nanoparticles (Fig. 1), block copolymers consisting of polyethylene glycol and polyaspartate, so-called PEG-polyaspartate described previously [2–4,11], were used. PTX was incorporated into polymeric micelles formed by physical entrapment utilizing hydrophobic interactions between PTX and the block copolymer polyaspartate chain. After screening of many candidate substances, 4-phenyl-1-butanol was employed for the chemical modification of the polyaspartate block to increase its hydrophobicity. Treating with a condensing agent, 1,3-diisopropylcarbodiimide, the half of carboxyl groups on the polyaspartate were esterified with 4-phenyl-1-butanol. Molecular weight of the polymers was determined to be approximately 20,000, (PEG block: 12,000; modified polyaspartate block: 8000). NK105 was prepared by facilitating the self-association of NK105 polymers and PTX. NK105 was obtained as a freeze-dried formulation and contained ca. 23% (w/w) of PTX, as determined by reversed-phase liquid-chromatography using an ODS column with mobile

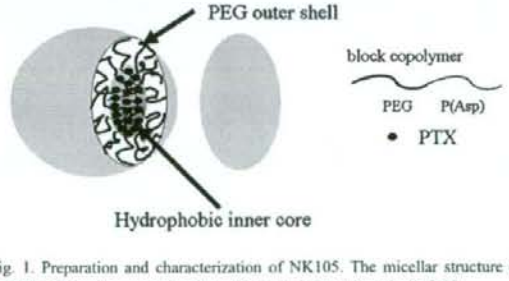

Fig. 1. Preparation and characterization of NK105. The micellar structure of NK105 PTX was incorporated into the inner core of the micelle [29].

Table 1
Pharmacokinetic parameters for the plasma and tumor concentrations of paclitaxel after single intravenous administration of NK105 and PTX to colon 26-bearing CDF1 mice

	Treatment	Dose (mg/kg)	$C_{5\ min}$ (μg/mL)	$t_{1/2z}$ (h)	AUC_{0-t} (μg·h/mL)	AUC_{0-inf} (μg·h/mL)	CL_{tot} (mL/h/kg)	V_{ss} (mL/kg)
Plasma	PTX	50	59.32	0.98	90.2[a)]	91.3	547.6	684.6
	PTX	100	157.67	1.84	309.0[b)]	309.0	323.6	812.2
	NK105	50	1157.03	5.99	7860.9[c)]	7862.3	6.4	46.4
	NK105	100	1812.37	6.82	15565.7[c)]	15573.6	6.4	54.8
			C_{max} (μg/mL)	T_{max} (h)	$t_{1/2z}$ (h)	AUC_{0-t} (μg·h/mL)		AUC_{0-inf} (μg·h/mL)
Tumor	PTX	50	12.50	2.0	7.02	120.8[b)]		133.0
	PTX	100	28.57	0.5	8.06	330.4[c)]		331.0
	NK105	50	42.45	24.0	35.07	2360.1[c)]		3192.0
	NK105	100	71.09	6.0	73.66	3884.9[c)]		7964.5

a) $AUC_{0-6\ h}$; b) $AUC_{0-24\ h}$; c) $AUC_{0-72\ h}$.
Parameters were calculated from the mean value of three or two mice by noncompartmental analysis [12].

phase consisting of acetonitrile and water (9:11, v/v) and detection of ultraviolet absorbance at 227 nm. Finally, NK105, a PTX-incorporating polymeric micellar nanoparticle formulation with a single and narrow size distribution, was obtained. The weight-average diameter of the nanoparticles was approximately 85 nm ranging from 20 to 430 nm [12].

2.2. Pharmacokinetics and pharmacodynamics of NK105

Colon 26-bearing CDF1 mice were given a single i.v. injection of PTX 50 or 100 mg/kg, or of NK105 at an equivalent dose of PTX. Subsequently, the time-course changes in the plasma and tumor levels of PTX were determined in the PTX and NK105 administration groups ; furthermore, the pharmacokinetic parameters of each group were also determined (Table 1). NK105 exhibited slower clearance from the plasma than PTX, while NK105 was present in the plasma for up to 72 h after injection; PTX was not detected after 24 h or later of injection. The plasma concentration at 5 min ($C_{5\ min}$) and the AUC of NK105 were 11- to 20-fold and 50- to 86-fold higher for NK105 than for PTX, respectively. Furthermore, the half-life at the terminal phase ($t_{1/2z}$) was 4 to 6 times longer for NK105 than for PTX. The maximum concentration (C_{max}) and AUC of NK105 in Colon 26 tumors were approximately 3 times and 25 times higher for NK105 than for PTX, respectively. NK105 continued to accumulate in the tumors until 72 h after injection. The tumor PTX concentration was higher than 10 μg/g even at 72 h after the intravenous injection of NK105 50 and 100 mg/kg. By contraries, the tumor PTX concentrations at 72 h after the intravenous administration of free PTX 50 and 100 mg/kg were below detection limits and less than 0.1 μg/g, respectively.

2.3. In vivo antitumor activity

BALB/c mice bearing s.c. HT-29 colon cancer tumors showed decreased tumor growth rates after the administration of PTX and NK105. However, NK105 exhibited superior antitumor activity as compared with PTX ($P<0.001$). The antitumor activity of NK105 administered at a PTX-equivalent dose of 25 mg/kg was comparable to that obtained after the administration of free PTX 100 mg/kg. Tumor suppression by NK105 increased in a dose-dependent manner. Tumors disappeared after the first dosing to mice treated with NK105 at a PTX-equivalent dose of 100 mg/kg, and all mice remained tumor-free thereafter (Fig. 2). In addition, less weight loss was induced in mice which were given NK105 100 mg/kg than in those which were given the same dose of free PTX(data not shown).

2.4. Neurotoxicity of PTX and NK105

Treatment with PTX has resulted in cumulative sensory-dominant peripheral neurotoxicity in humans, characterized clinically by numbness and/or paraesthesia of the extremities. Pathologically, axonal swelling, vesicular degeneration, and demyelination were observed. We, therefore, examined the effects of free PTX and NK105 using both electrophysiological and morphological methods.

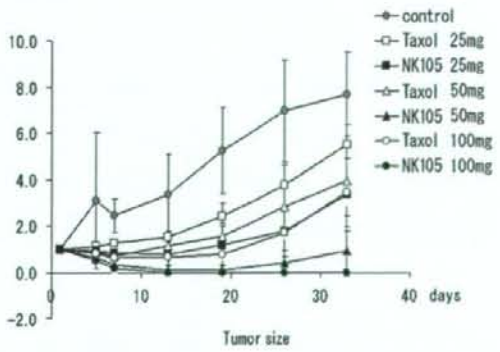

Fig. 2. Effects of PTX (open symbols) and NK105 (closed symbols). PTX and NK105 were injected intravenously once weekly for 3 weeks at PTX-equivalent doses of 25 mg/kg (□, ■), 50 mg/kg (△, ▲), and 100 mg/kg (○, ●), respectively. Saline was injected to animals in the control group (◉) [12].

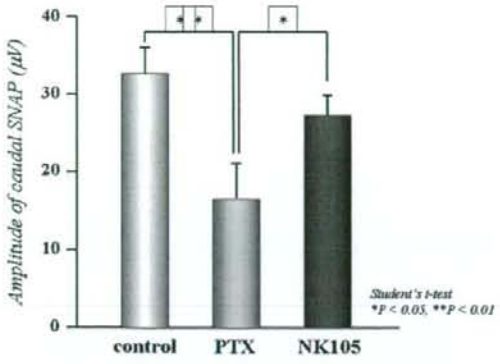

Fig. 3. Effects of PTX or NK105 on the amplitude of rat caudal sensory nerve action potentials as examined 5 days after weekly injections for 6 weeks. Rats ($n=14$) were injected with NK105 or PTX at a PTX-equivalent dose of 7.5 mg/kg. 5% glucose was also injected in the same manner to animals in the control group [12].

Prior to drug administration, there were no significant differences in the amplitude of caudal sensory nerve action potential (caudal SNAP) between two drug administration groups. On day 6 after the last dosing (at week 6), the amplitude of the caudal SNAP in the control group increased in association with rat maturation. The amplitude was significantly smaller in the PTX group than in the control group ($P<0.01$), while the amplitude was significantly larger in the NK105 group than in the PTX group ($P<0.05$) and was comparable between the NK105 group and the control group (Fig. 3). Histopathological examination of longitudinal paraffin-embedded sections of the sciatic nerve 5 days after the sixth weekly injection revealed degenerative changes. The NK105 administration group showed only a few degenerative myelinated fibers in contrast to the PTX administration group which indicated markedly more numerous degenerative myelinated fibers (data not shown).

2.5. NK105 has more potent radiosensitizing effect than free paclitaxel

Besides the antitumor activity of PTX, its ability to induce radiosensitization has been reported both in vitro [13–16] and *in vivo* [17–19] this effect has been attributed to its effect of stabilizing microtubules and inducing cell cycle arrest at the G2/M phase, the most radiosensitive phase of the cell cycle [20,21]. Since several clinical studies have demonstrated the efficacy of PTX-based chemotherapy combined with radiotherapy, the combined modality is considered to be a potentially important treatment option for lung and breast cancer [22,23].

The adverse effects of radiation, namely, lung toxicities in patients with breast or lung cancer treated by thoracic radiation,

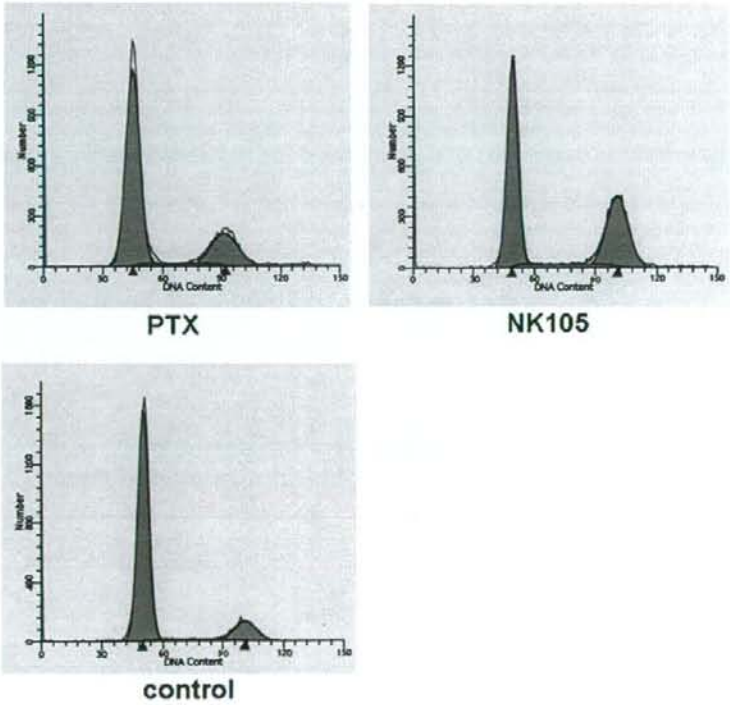

Fig. 4. Cell cycle analysis. Cell cycle analysis of LLC tumor cells 24 h after adding saline as a control, PTX or NK105 [28].

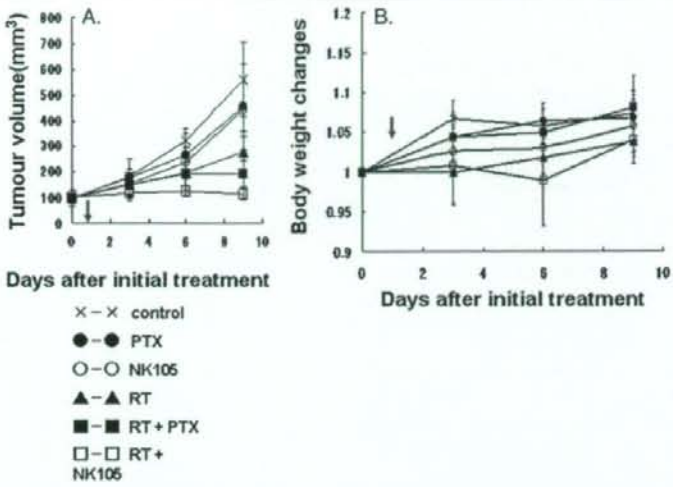

Fig. 5. Antitumor activity. Changes in the LLC tumor growth rates in the mice. (A) Mice receiving TXL-alone(●), NK105-alone(○), combined treatment with PTX and radiation(■), and combined treatment with NK105 and radiation(□) were administered a single i.v. injection of PTX or NK105 at the dose 45 mg/kg. Twenty-four hours after the drugs were administered, the mice in the radiation-alone (Δ)and the combined-treatment groups were irradiated. Mice in the control group (X) were given no treatment. (B) Changes in the relative body weight. Data were derived from the same mice as those used in the present study [28].

are of great concern, and may be dose-limiting or even have a negative impact on the quality of life of the patients, even though radiation is an efficient treatment option. Lung toxicities often result in lung fibrosis, necessitating change of the treatment method and causing much distress or even death of the patients [24,25]. Some clinical trials actually reported an increased incidence of pneumonitis following combined PTX therapy with radiation in patients with breast or lung cancer [26,27].

It is expected that the use of NK105 in place of PTX in combination with radiation may also yield superior results, because of the more potent antitumor activity of this drug as compared to that of free PTX. We evaluated the antitumor activity and severity of lung fibrosis induced by PTX and NK105 administered in combination with thoracic radiation, to examine whether combined NK105 chemotherapy with radiation would be an acceptable or useful treatment modality.

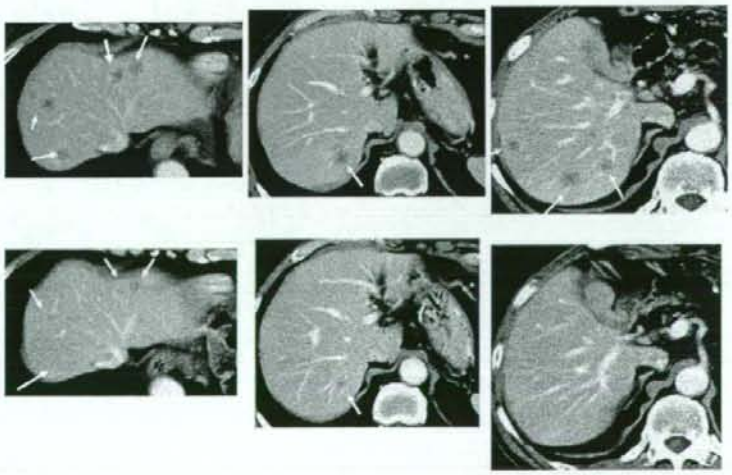

Fig. 6. Serial CT scans. A 60-year-old male with pancreatic cancer who was treated with NK105 at a dose level of 150 mg/m^2. Baseline scan (upper panels) showing multiple metastasis in the liver. Partial response, characterized by a more than 90% decrease in the size of the liver metastasis (lower panels) compared with the baseline scan. The antitumor response was maintained for nearly 1 year [29].

2.5.1. Cell cycle analysis

At 24 h after the administration of PTX or NK105 to the LLC-tumor-bearing mice, severe cell cycle arrest at the G2/M phase was observed in the tumor cells treated with the drugs as compared with that in the control (no drug treatment). There was a tendency towards the NK105-treated LLC tumor cells showing more severe arrest at the G2/M phase than the PTX-treated cells [28] (Fig. 4).

2.5.2. Antitumor activity

Decreased tumor growth rates of the LLC tumors were observed in the mice of the radiation alone, combined PTX with radiation, and combined NK105 with radiation groups [28]. No antitumor activity was observed following treatment with either PTX or NK105 alone, because LLC is primarily a PTX-resistant tumor. Combined NK105 therapy with radiation yielded superior antitumor activity as compared to both radiation alone ($P=0.0047$) and combined PTX therapy with radiation ($P=0.0277$) on the day 9 after the treatment initiation (Fig. 5A). No significant differences in body weight changes were noted among the groups tested (Fig. 5B).

2.5.3. Lung toxicities

Histopathological examination of the lung sections of all the mice receiving radiation showed inflammatory cell infiltration, appearance of intra-alveolar macrophages, and destruction of the alveolar architecture. Major portions of the alveolar septa in the lung sections prepared from the irradiated mice showed slight thickening, although no massive structural destruction was observed. On the other hand, the lung sections prepared from the control non-irradiated group showed no significant histopathological changes. Ashcroft's fibrosis scores in the groups of mice that received radiation ranged from 0.975 to 1.426, with no significant differences among the groups. The score in the control group was nearly zero. In the groups receiving radiation, the severity of lung fibrosis differed significantly among the mice within the same groups, as did the Ashcroft's scores, that is, the S.D. of the Ashcroft's scores in the mice receiving radiation was very high.

2.6. Clinical study

A phase I study was designed to determine maximum tolerated dose (MTD), dose-limiting toxicities (DLTs), the recommended dose (RD) for phase II and the pharmacokinetics of NK105 [29].

NK105 was administered by a 1-hour intravenous infusion every 3 weeks without anti-allergic premedication. The starting dose was 10 mg PTX equivalent/m^2, and dose escalated according to the accelerated titration method.

To date, 17 patients (pts) have been treated at the following doses: 10 mg/m^2 ($n=1$); 20 mg/m^2 ($n=1$); 40 mg/m^2 ($n=1$); 80 mg/m^2 ($n=1$); 110 mg/m^2 ($n=3$); 150 mg/m^2 ($n=5$); 180 mg/m^2 ($n=5$). Tumor types treated have included: pancreatic ($n=9$), bile duct ($n=5$), gastric ($n=2$), and colon ($n=1$). Neutropenia has been the predominant hematological toxicity and grade 3 or 4 neutropenia was observed in pts treated at 110, 150 and 180 mg/m^2. One patient at 180 mg/m^2 developed grade 3 fever. No other

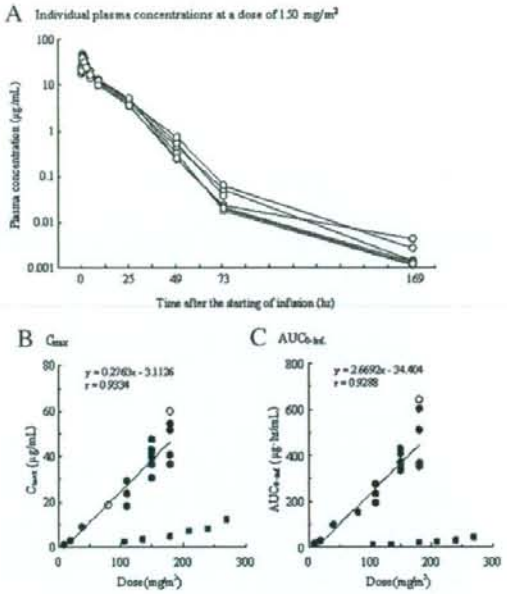

Fig. 7. (A) Individual plasma concentrations of PTX in 7 patients following 1 h intravenous infusion of NK105 at a dose of 150 mg/m^2. Relationships between dose and C_{max} (B), and between dose and AUC_{0-inf}. (C) of PTX in patients following 1 h intravenous infusion of NK105. Regression analysis for dose vs. C_{max} was applied using all points except one patient at 80 mg/m^2 whose medication time became 11 min longer and one patient at 180 mg/m^2 who had medication discontinuation and steroid medication. (○) Regression analysis for dose vs. AUC_{0-inf} was applied using all points except one patient who had medication discontinuation and steroid medication. (○) Relationships between dose and C_{max}, and AUC_{0-inf} in patients following conventional PTX administration were plotted (closed square) [29].

grade 3 or 4 non-hematological toxicity including neuropathies was observed. DLTs were observed in pts with at the 180 mg/m^2 (grade 4 neutropenia lasting for more than 5 days), which was determined as MTD. Allergic reactions were not observed in any of the patients except one patient at level. A partial response was observed in one pancreatic cancer pt who received more than 12 courses of NK105 (Fig. 6). Despite of the long time usage, only grade 1 or 2 neuropathy was observed by modifying the dose or period of drug administration. Colon and gastric cancer pts experienced stable disease lasting 10 and 7 courses, respectively. The C_{max} and AUC of NK105 showed dose-dependent characteristics. The plasma AUC of NK105 at 180 mg/m^2 was approximately 30-fold higher than that of commonly-used paclitaxel formulation (Fig. 7).Accrual is ongoing at the 150 mg/m^2 dose level to determine RD. DLT was Grade 4 neutropenia. NK105 generates prolonged systemic exposure to PTX in plasma. Tri-weekly 1-hour infusion of NK105 was feasible and well tolerated, with antitumor activity in pancreatic cancer pt. A phase 2 study of NK105 against stomach cancer is now underway.

3. NC-6004, cisplatin-incorporating micellar nanoparticle

Cisplatin [*cis*-dichlorodiammineplatinum (II): CDDP] is a key drug in the chemotherapy for cancers, including lung,

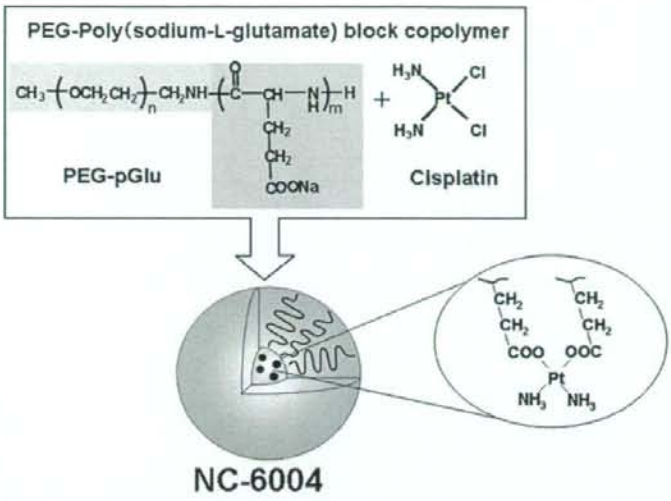

Fig. 8. Preparation and characterization of cisplatin-incorporating polymeric micelles (NC-6004). Chemical structures of cisplatin (CDDP) and polyethylene glycol poly(glutamic acid) block copolymers [PEG-P(Glu) block copolymers], and the micellar structures of CDDP-incorporating polymeric micelles (NC-6004) [39].

gastrointestinal, and genitourinary cancer [30,31]. However, we often find that it is necessary to discontinue treatment with CDDP due to its adverse reactions, e.g., nephrotoxicity and neurotoxicity, despite its persisting effects [32]. Platinum analogues, e.g., carboplatin and oxaliplatin [33], have been developed to date to overcome these CDDP-related disadvantages. Consequently, these analogues are becoming the standard drugs for ovarian cancer [34] and colon cancer [35]. However, those regimens including CDDP are considered to constitute the standard treatment for lung cancer, stomach cancer, testicular cancer [36], and urothelial cancer [37]. Therefore, the development of a drug delivery system (DDS) technology is anticipated, which would offer the better selective accumulation of CDDP into solid tumors while lessening its distribution into normal tissue.

3.1. Preparation and characterization of NC-6004

NC-6004 were prepared according to the slightly modified procedure reported by Nishiyama et al. [38,39] (Fig. 8). NC-6004 consists of polyethylene glycol (PEG), a hydrophilic chain which constitutes the outer shell of the micelles, and the coordinate complex of poly(glutamic acid) (P(Glu)) and CDDP, a polymer–metal complex-forming chain which constitutes the inner core of the micelles. The molecular weight of PEG-P(Glu) as a sodium salt was approximately 18,000 (PEG: 12,000; P(Glu): 6000). The CDDP-incorporated polymeric micelles were clearly discriminated from typical micelles from amphiphilic block copolymers. The driving force of the formation of the CDDP-incorporated micelles is the ligand substitution of platinum(II) atom from chloride to carboxylate in the side chain of P(Glu). The molar ratio of CDDP to the carboxyl groups in the copolymers was 0.71 [38]. A narrowly distributed size of polymeric micelles (30 nm) was confirmed by the dynamic light scattering (DLS) measurement. Also, the static light scattering (SLS) measurement revealed that the CDDP-loaded micelles showed no dissociation upon dilution and the CMC was less than 5×10^{-7}, suggesting remarkable stability compared with typical micelles from amphiphilic block copolymers [38]. It is assumed that the interpolymer cross-linking by Pt(II) atom might contribute to stabilization of the micellar structure.

Table 2
Pharmacokinetic parameter estimates for CDDP and NC-6004 in rats

Compound	Rat	T^a_{max} (h)	C^a_{max} (mg/mL)	$t_{1/2z}$ (h)	AUC_{0-t} (mg h/mL)	AUC_{0-inf} (mg h/mL)	CL_{tot} (mL/h/kg)	MRT_{0-inf} (h)	V_{ss} (L/kg)
CDDP	Mean	0.083	11.67	34.50	20.47	75.73	70.67	46.57	3.00
	S.D.		0.57	16.14	2.25	26.13	20.34	22.38	0.61
NC-6004	Mean	0.50	89.90	6.43	1325.90	1335.47	3.77	10.67	0.04
	S.D.		4.29	0.55	77.85	75.99	0.21	0.15	0.0023

See text for definitions of parameters.
The pharmacokinetic parameters were calculated after fitting to a non compartment model using WinNonlin program.
[a]For CDDP group, values of T_{max} and C_{max} represent 5 min and $C_{5\ min}$, respectively [39].

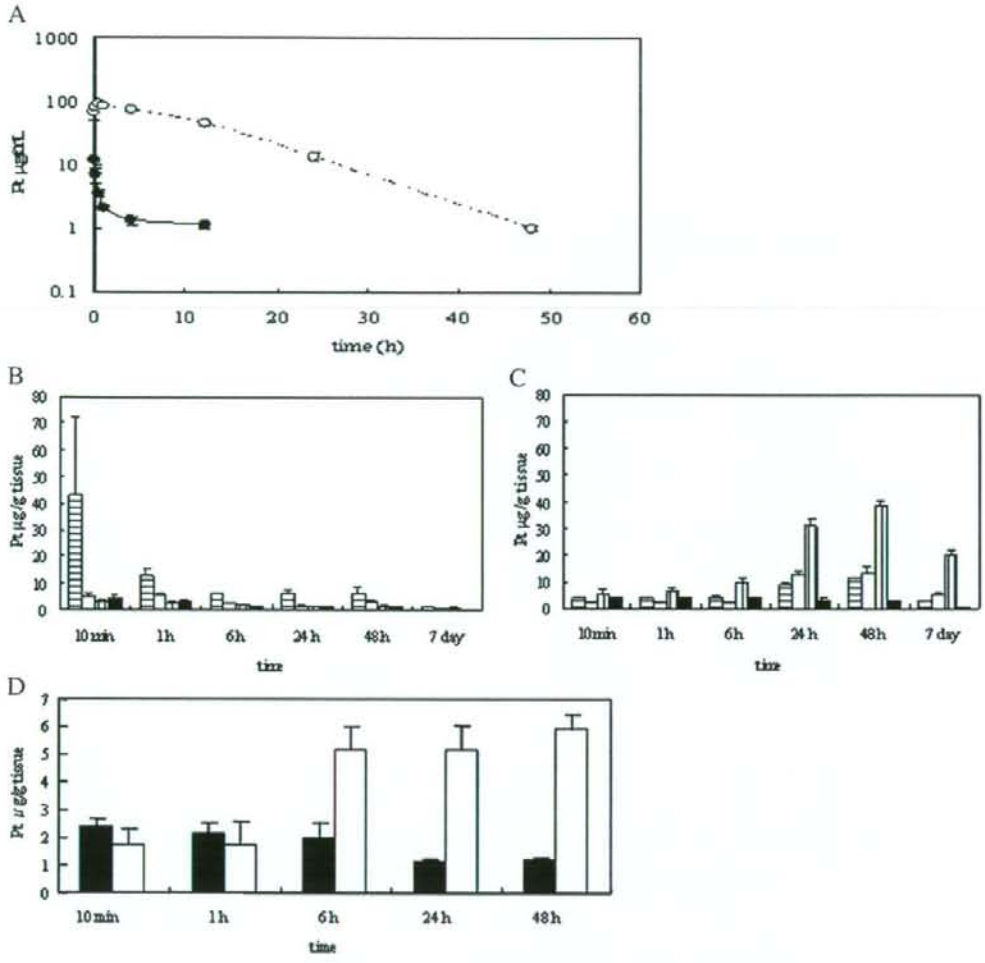

Fig. 9. Time profiles of platinum (Pt) concentration in the plasma and tissue distribution of Pt after a single i.v. injection of CDDP (5 mg/kg) or NC-6004 (an equivalent dose of 5 mg/kg CDDP). (A) Concentration-time profile of Pt in the plasma after a single i.v. injection of CDDP (●) and NC-6004 (○) in rats ($n=3$). Tissue distribution of platinum after a single i.v. injection of CDDP (B) and NC-6004 (C) in rats ($n=3$) (kidney (▥), liver (□), spleen (▤), and lung (■)). (D) Time profiles of platinum concentration in the MKN-45 solid tumor after a single i.v. injection of CDDP (■) and NC-6004 (□) in MKN-45 bearing BALB/c nude mice ($n=3$). Values are expressed as the mean±S.D [39].

The release rates of CDDP from NC-6004 were 19.6% and 47.8% at 24 and 96 h, respectively. In distilled water, furthermore, NC-6004 was stable without releasing cisplatin.

3.2. Pharmacokinetics and pharmacodynamics

FAAS could measure serum concentrations of platinum up to 48 h after i.v. injection of NC-6004 but could measure them only up to 4 h after i.v. injection of CDDP. NC-6004 showed a very long blood retention profile as compared with CDDP [39]. The AUC_{0-t} and C_{max} values were significantly higher in animals given NC-6004 than in animals given CDDP, namely, 65-fold and 8-fold, respectively ($P<0.001$ and $P<0.001$, respectively) (Table 2, Fig. 9A). Furthermore, the CL_{tot} and V_{ss} values were significantly lower in animals given NC-6004 than in animals given CDDP, i.e., one-nineteenth and one-seventy fifth, respectively ($P<0.01$ and $P<0.01$, respectively) (Table 2).

Regarding the concentration-time profile of platinum in various tissues after i.v. injection of CDDP or NC-6004, all organs measured exhibited the highest concentrations of platinum within 1 h after administration in all animals given CDDP (Fig. 9B). Furthermore, animals given NC-6004 exhibited the highest tissue concentrations of platinum in the liver and spleen at late time points (24 and 48 h after administration, respectively). However, the concentrations decreased on day 7 after administration (Fig. 9C). In addition, and in a similar manner to other drugs which are incorporated in polymeric carriers, NC-6004 demonstrated accumulation in organs of the

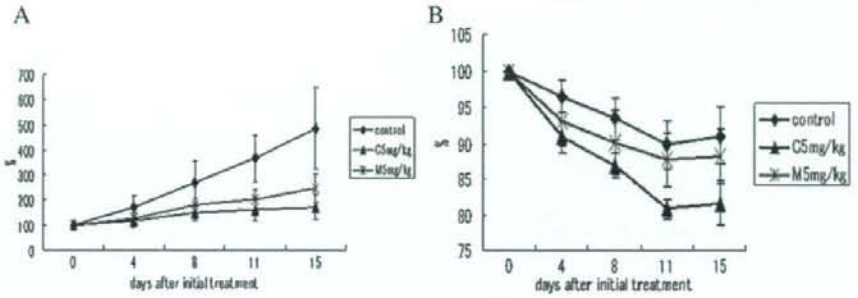

Fig. 10. Relative changes in MKN-45 tumor growth rates in nude mice. (A) CDDP(▲) and NC-6004(X) were injected intravenously every 3 days, 3 administrations in total, at CDDP-equivalent doses of 5 mg/kg. 5% glucose was injected in the control mice (◇). (B) Changes in relative body weight. Data were derived from the same mice as those used in the present study. Values are expressed as the mean±S.E [39].

reticuloendothelial system, e.g., liver and spleen. At 48 h after administration, tissue concentrations of platinum in the liver and spleen were 4.6- and 24.4-fold higher for NC-6004 than for CDDP. On the other hand, a marked increase in tissue platinum concentration was observed immediately after administration in the kidneys of animals given CDDP. Renal platinum concentration at 10 min and 1 h after administration were 11.6- and 3.1-fold lower, respectively, in animals given NC-6004 than in animals given CDDP. Furthermore, the maximum concentration (C_{max}) in the kidney was 3.8-fold lower at the time of NC-6004 administration than at the time of CDDP administration.

Regarding the tumor accumulation of platinum, tumor concentrations of platinum peaked at 10 min after administration of CDDP. On the other hand, tumor concentrations of platinum peaked at 48 h after administration of NC-6004 (Fig. 9D). The maximum concentration (C_{max}) in tumor was 2.5-fold higher for NC-6004 than for CDDP ($P<0.001$). Furthermore, the tumor AUC was 3.6-fold higher for NC-6004 than for CDDP (81.2 μg/mL h and 22.6 μg/mL h in animals given NC-6004 and CDDP, respectively).

3.3. In vivo antitumor activity

BALB/c nude mice implanted with a human gastric cancer cell line MKN-45 showed decreased tumor growth rates after i.v. injection of CDDP and NC-6004 (Fig. 10A). In the administration of CDDP, the CDDP 5 mg/kg administration group showed a significant decrease ($P<0.01$) in tumor growth rate as compared with the control group. However, the NC-6004 administration groups at the same dose levels as CDDP showed no significant difference in tumor growth rate. Regarding time-course changes in body weight change rate, the CDDP 5 mg/kg administration group showed a significant decrease ($P<0.001$) in body weight as compared with the control group. On the other hand, NC-6004 administration group did not show a decrease in body weight as compared with the control group (Fig. 10B).

3.4. Nephrotoxicity of CDDP and NC-6004

In the CDDP 10 mg/kg administration group, 4 of 12 rats died from toxicity within 7 days after drug administration. No deaths occurred in the NC-6004 10 mg/kg administration group. Regarding renal function, the BUN concentrations on day 7 after the administration of 5% glucose, CDDP 10 mg/kg, and NC-6004 10 mg/kg were 20.8±3.0, 65.3±44.4, and 20±4.5 mg/dL, respectively. The plasma concentrations of creatinine on day 7 after the administration of 5% glucose, CDDP 10 mg/kg, and NC-6004 10 mg/kg were 0.27±0.03, 0.68±0.23, and 0.28±0.04 mg/dL, respectively. The CDDP 10 mg/kg administration group showed significantly higher plasma concentrations of BUN and creatinine as compared with the control group ($P<0.05$ and $P<0.001$, respectively), with the NC-6004 10 mg/kg administration group ($P<0.05$ and $P<0.001$, respectively) (Fig. 11A and B). Light microscopy indicated tubular dilation with flattening of the lining cells of the tubular epithelium in the kidney from all animals in the CDDP 10 mg/kg administration group. On the other hand, no histopathological change was observed in the kidneys from all animals in the NC-6004 10 mg/kg administration group.

3.5. Neurotoxicity of CDDP and NC-6004

Neurophysiological examination revealed that motor nerve conduction velocities (MNCVs) in animals given 5% glucose, CDDP, and NC-6004 were 44.2±3.5, 40.94±5.08, and 40.62±0.63 m/s, respectively. No significant difference was found among the groups with respect to MNCV. Furthermore, sensory

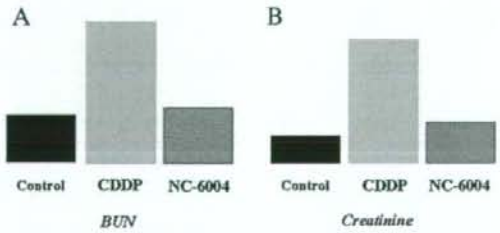

Fig. 11. Nephrotoxicity of CDDP and NC-6004. Plasma concentrations of blood urea nitrogen (BUN) and creatinine were measured after a single i.v. injection of 5% glucose ($n=8$), CDDP at a dose of 10 mg/kg ($n=12$), NC-6004 at a dose of 10 mg/kg ($n=13$) on a CDDP basis (modification of ref. [39]).

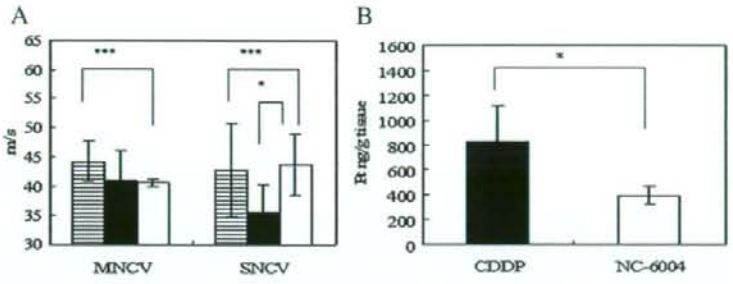

Fig. 12. Neurotoxicity of CDDP and NC-6004 in rats. Rats ($n=5$) were given CDDP (2 mg/kg), NC-6004 (an equivalent dose of 2 mg/kg CDDP), or 5% glucose, all intravenously twice a week, 11 administrations in total. Sensory nerve conduction velocity (SNCV) and motor nerve conduction velocity (MNCV) of the sciatic nerve at week 6 after the initial administration (A). The platinum concentration in the sciatic nerve. Rats were given CDDP (5 mg/kg, $n=5$), NC-6004 (an equivalent dose of 5 mg/kg CDDP, $n=5$), or 5% glucose ($n=2$), all intravenously twice a week, 4 administrations in total. On day 3 after the final administration, a segment of the sciatic nerve was removed and the platinum concentration in the sciatic nerve was measured by ICP-MS (B). The data are expressed as the mean±S.D. *: $P<0.05$ [39].

nerve conduction velocities (SNCVs) in animals given 5% glucose, CDDP, and NC-6004 were 42.86±8.07, 35.48±4.91, and 43.74±5.3 m/s, respectively. Animals given NC-6004 showed no delay in SNCV as compared with animals given 5% glucose. On the other hand, animals given CDDP showed a significant delay ($P<0.05$) in SNCV as compared with animals given NC-6004 (Fig. 12A). The analysis by ICP-MS on sciatic nerve concentrations of platinum could not detect platinum in the sciatic nerve from animals given 5% glucose (data not shown). Sciatic nerve concentrations of platinum in animals given CDDP and NC-6004 were 827.2±291.3 and 395.5± 73.1 ng/g tissue. Therefore, the concentrations were significantly ($P<0.05$) lower in animals given NC-6004 (Fig. 12B). This finding is believed to be a factor which reduced neurotoxicity following NC-6004 administration as compared with the CDDP administration.

3.6. Present situation of a clinical study of NC-6004

A phase 1 clinical trial of NC-6004 is now under way in United Kingdom. Starting dose of NC-6004 was 10 mg/m2. NC-6004 was administered once every 3 weeks with only 1000 ml water loading. In Japan, a phase 1 trial will be stared soon in the National Cancer Center Hospital.

4. NK012, SN-38-incorporating micellar nanoparticle

The antitumor plant alkaloid camptothecin (CPT) is a broad-spectrum anticancer agent which targets the DNA topoisomerase I. Although CPT has showed promising antitumor activity *in vitro* and *in vivo* [40,41], it has not been used clinically because of its low therapeutic efficacy and severe toxicity [42,43]. Among CPT analogs, irinotecan hydrochloride (CPT-11) has recently been demonstrated to be active against colorectal, lung, and ovarian cancer [44–48]. CPT-11 itself is a prodrug and is converted to 7-ethyl-10-hydroxy-CPT (SN-38), a biologically active metabolite of CPT-11, by carboxylesterases (CEs). SN-38 exhibits up to 1000-fold more potent cytotoxic activity against various cancer cells *in vitro* than CPT-11 [49]. Although CPT-11 is converted to SN-38 in the liver and tumor, the metabolic conversion rate is less than 10% of the original volume of CPT-11 [50,51]. In addition, the conversion of CPT-11 to SN-38 depends on the genetic inter-individual variability of CE activity [52]. Thus, direct use of SN-38 might be of great advantage and attractive for cancer treatment. For the clinical use of SN-38, however it is essential to develop a soluble form of water-insoluble SN-38. The progress of the manufacturing technology of "micellar nanoparticles" may make it possible to use SN-38 for *in vivo* experiments and further clinical use.

4.1. Preparation and characterization of NK012

NK012 is an SN-38-loaded polymeric micelle constructed in an aqueous milieu by the self-assembly of an amphiphilic block copolymers, PEG-PGlu(SN-38) [53]. The molecular weight of PEG-PGlu(SN-38) was determined to be approximately 19,000 (PEG segment: 12,000; SN-38-conjugated PGlu segment: 7,000). NK012 was obtained as a freeze-dried formulation and contained ca. 20% (w/w) of SN-38 (Fig. 13A). The mean particle size of NK012 is 20 nm in diameter with a relatively narrow range (Fig. 13B). The releasing rates of SN-38 from NK012 in phosphate buffered saline at 37 °C were 57% and 74% at 24 h and 48 h, respectively, and that in 5% glucose solution at 37 °C were 1% and 3% at 24 h and 48 h, respectively (Fig. 13C). These results indicate that NK012 can release SN-38 under neutral condition even without the presence of a hydrolytic enzyme, and is stable in 5% glucose solution. It is suggested that NK012 is stable before administration and starts to release SN-38, the active component, under physiological conditions after administration.

4.2. Cellular sensitivity of NSCLC and colon cancer cells to SN-38, NK012, and CPT-11

The IC_{50} values of NK012 for the cell lines ranged from 0.009 μM (Lovo cells) to 0.16 μM (WiDR cells). The growth-inhibitory effects of NK012 are 43–340-fold more potent than those of CPT-11, whereas the IC_{50} values of NK012 were 2.3–5.8-fold higher than those of SN-38.NK012 exhibited a higher

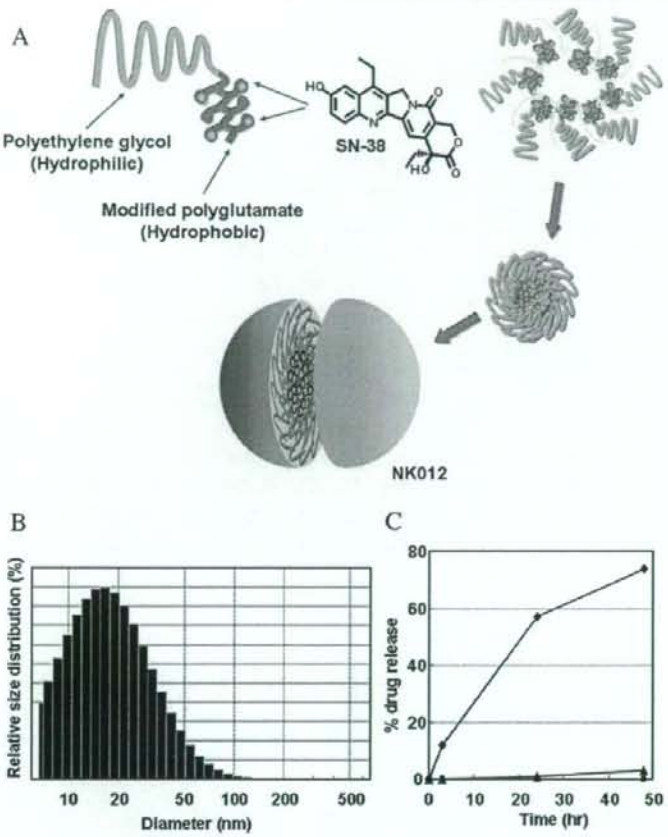

Fig. 13. Schematic structure of NK012. A polymeric micelle carrier of NK012 consists of a block copolymer of PEG (molecular weight of about 5000) and partially modified polyglutamate (about 20 unit). Polyethylene glycol (hydrophilic) is believed to be the outer shell and SN-38 was incorporated into the inner core of the micelle [56].

cytotoxic effect against each cell line as compared with CPT-11 (×43–340-fold sensitivity). On the other hand, the IC_{50} values of NK012 were a little higher than those of SN-38, similar to the cytotoxic feature also reported in a previous study about micellar drugs [39].

4.3. Pharmacokinetic analysis of NK012 and CPT-11 using HT-29-bearing nude mice

After injection of CPT-11, the concentrations of CPT-11 and SN-38 for plasma declined rapidly with time in a log–linear

Table 3
Tumor-to-plasma concentration ratio (Kp) of analytes after an intravenous administration of NK012 (30 mg/kg) to nude mice bearing human colon cancer HT-29

Test article	Analyte		Time after administration (h)						
			0.0833	1	6	24	48	72	168
NK012	P-b SN-38*	Plasma (μg/mL)	612	410	254	23.3	1.25	0.278	0.0333
		Tumor (μg/g)	4.99	8.00	13.8	9.95	5.90	5.03	3.58
		Kp (mL/g)‡	0.00815	0.0195	0.0543	0.427	4.72	18.1	108
	P-u SN-38†	Plasma (μg/mL)	3.10	1.24	0.673	0.0717	0.0127	0.00925	0.00325
		Tumor (μg/g)	0.0763	0.187	0.188	0.0904	0.0531	0.0426	0.0358
		Kp (mL/g)‡	0.0246	0.151	0.279	1.26	4.18	4.61	11.0

NOTE: Data were expressed as means of three mice [56]. * Ploymer-bound SN-38; SN-38 remaining bound to PEG-PGlu. †Polymer-unbound SN-38; free SN-38 from PEG-PGlu. ‡Kp values were calculated on the mean concentrations of three mice.

A

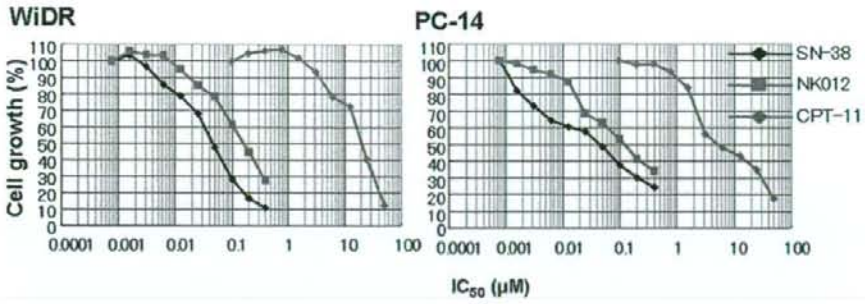

cell line	SN-38	NK012	CPT-11
WiDR	0.046 ± 0.008	0.16 ± 0.014	20.4 ± 1.6
SW480	0.025 ± 0.003	0.11 ± 0.028	31.9 ± 1.3
Lovo	0.0067 ± 0.0012	0.026 ± 0.003	7.24 ± 1.04
HT-29	0.016 ± 0.003	0.068 ± 0.007	23.1 ± 2.63
PC-14	0.044 ± 0.025	0.14 ± 0.021	5.96 ± 0.90
SBC-3	0.0016 ± 0.001	0.0093 ± 0.005	0.72 ± 0.22
A431	0.0081 ± 0.002	0.019 ± 0.007	5.6 ± 1.5

B

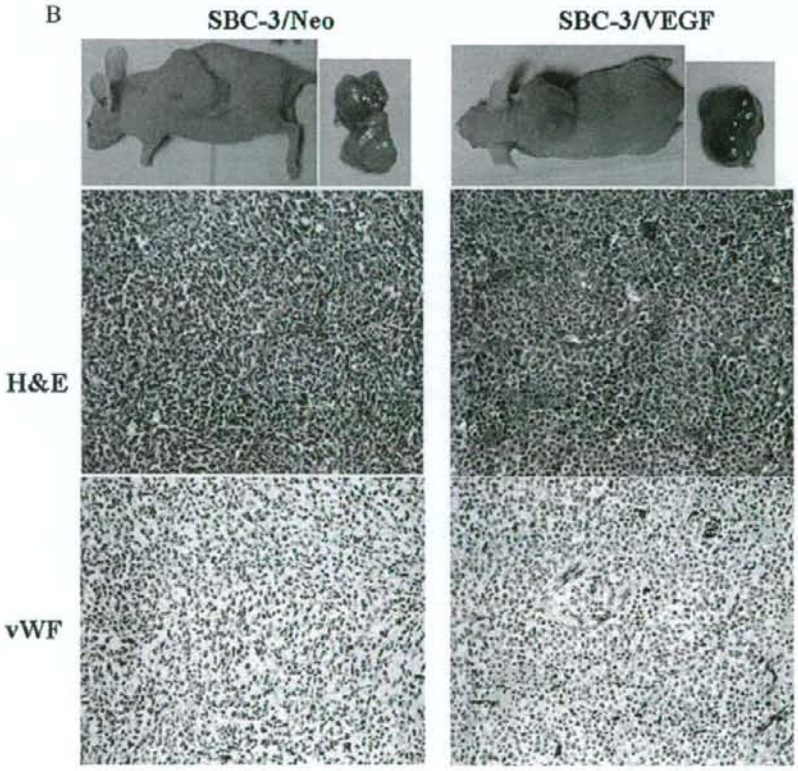

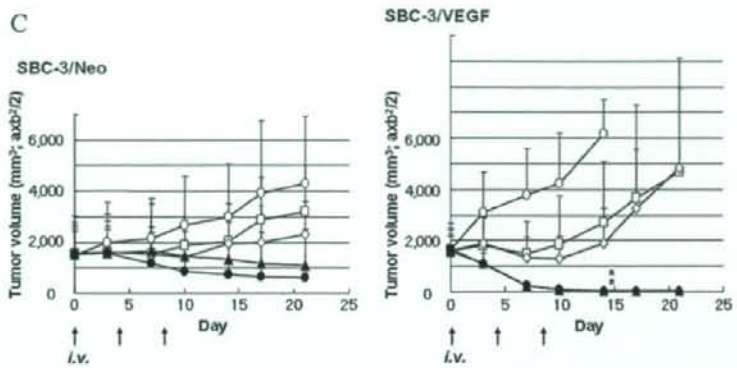

Fig. 14. Growth-inhibitory effect of NK012, SN-38, and CPT-11 on SBC-3/Neo and SBC-3/VEGF cells. (A) In *in vitro* experiment, the cells were exposed to the indicated concentrations of each drug for 72 h. The growth–inhibition curves and IC_{50} values for NK012 (▲), SN-38 (♦), and CPT-11 (■) are shown. (B) Representative photographs of massive tumors developed from SBC-3/Neo and SBC-3/VEGF at the time just before treatment initiation. Histological (H & E, ×20) and Immunohistochemical (vWF, ×20) examination for each tumor are shown. (C) Intravenous administration of NK012 or CPT-11 was started when the mean tumor volumes of groups reached a massive 1500 mm^3. The mice were divided into test group (○: control; □: CPT-11 20 mg/kg/day; ◇: CPT-11 40 mg/kg/day; ▲: NK012 15 mg/kg/day; and ●: NK012 30 mg/kg/day). NK012 or CPT-11 was administered *i.v.* on days 0, 4, and 8. Each group consisted of 4 mice. *$P<0.05$ [56].

fashion. On the other hand, NK012 (polymer-bound SN-38) exhibited slower clearance. The clearance of NK012 in the HT-29 tumor was significantly slower and the concentration of free SN-38 was maintained at more than 30 ng/g even at 168 h after injection. The pharmacokinetic parameters of each drug in the plasma and tumor are depicted in Table 3.

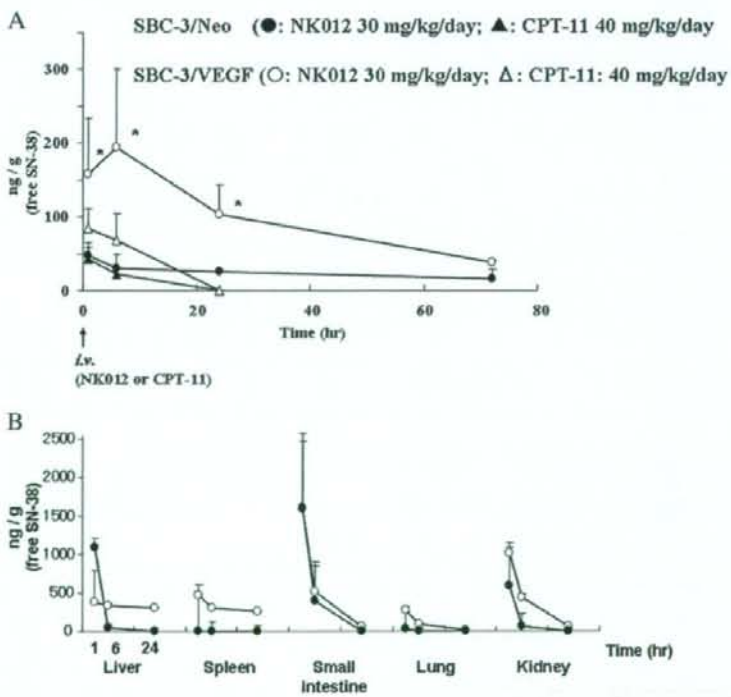

Fig. 15. Tissue and tumor distribution of free SN-38 after administration of NK012 and CPT-11. (A) Time profile of free SN-38 concentration in the SBC-3/Neo (●: NK012 30 mg/kg/day; ▲: CPT-11 40 mg/kg/day) and SBC-3/VEGF (○: NK012 30 mg/kg/day; Δ: CPT-11: 40 mg/kg/day). NK012 on day 0 and day 4 (96 h) or CPT-11 on day 0 were administered. *$P<0.05$. (B) Tissue distribution of free SN-38 after single injection of NK012 at 30 mg/kg (○) and CPT-11 at 40 mg/kg(●) [56].